



ELSEVIER

New Astronomy 3 (1998) 57–73

NEW
ASTRONOMY

1D gasdynamics of wind-blown bubbles: effects of thermal conduction

S.A. Zhekov^{a,1}, A.V. Myasnikov^{b,2}

^aSpace Research Institute, Bulgarian Academy of Sciences, 6 Moskovska str., Sofia 1000, Bulgaria

^bInstitute for Problems in Mechanics, Russian Academy of Sciences, 101 Vernadskii Ave., Moscow 117526, Russia

Received 22 July 1997; accepted 3 November 1997

Communicated by Richard McCray

Abstract

Gasdynamic properties of the wind-blown bubbles are considered in the framework of the 1D spherically symmetric flow. The model self-consistently takes into account the optically-thin-plasma cooling and the electron thermal conduction. The numerical method used in calculations is described in details. A comparison with the existing self-similar solution is provided. It is shown that the self-similar solution gives a relatively well representation of the hot-bubble interior and could be used for estimations of some of its spectral characteristics. However, it is also shown that the thermal conduction in combination with the cooling may cause additional multiple shocks to appear in the interaction region and the analysis of the nature of these shocks is provided. © 1998 Elsevier Science B.V.

PACS: 95.30.Lz; 97.10.Fy; 98.38.-j

Keywords: Hydrodynamics; Conduction; Shock waves; ISM: bubbles

1. Introduction

It is well known that one of the main properties of the hot luminous stars is the presence of stellar winds with relatively high mass loss rates and wind velocities (e.g., Conti & Underhill, 1988). Thus, these objects supply a considerable amount of mechanical energy into the neighbouring matter (circumstellar and interstellar gas) which leads to an active interaction with their surroundings. Since the stellar

winds from the luminous stars are highly supersonic, this interaction results in formation of so called wind-blown bubbles (WBB) around these objects which explains the nebulae having been observationally found in optical since relatively long time ago (e.g., Chu, 1981; Lozinskaya, 1982). On the other hand, the high velocities of the stellar winds suggest that the shocked gas in the WBB is heated to high temperatures and it will be a source of X-ray emission. It has to be mentioned that the X-ray studies of these objects can serve as an important tool for testing our knowledge about the shock formation in cosmic plasma.

¹E-mail: szhekov@bgearn.acad.bg

²E-mail: myas@ipmnet.ru

Unfortunately, only one object has been well studied in the X-rays so far, namely, this is NGC 6888 and one of the main results is that the temperature of the gas emitting in X-rays is considerably (from a few times to one order of magnitude) lower than that corresponding to the stellar wind velocity (Bochkarev, 1988; Wrigge et al., 1994). Such a discrepancy means that some additional mechanism should be taken into account in the physics of the WBB. A possible physical process which can effectively lower the WBB gas temperature is the thermal conduction. Its importance also follows from the fact that gases with very different temperature are in contact in the WBB interior. Namely, the shocked stellar wind gas is expected to be very hot since the wind velocities, correspondingly the shock velocities, are of the order of thousands km s^{-1} while the shocked interstellar gas has a temperature typical for the HII regions since it is photoionized by the UV emission of the central star.

Although the physical picture of the WBB has been a subject of active numerical modelling (e.g., Rozyczka, 1985; Rozyczka & Tenorio-Tagle, 1985a,b; D’Ercole, 1992; Brighenti & D’Ercole, 1995a,b, 1997; Garcia-Segura & Mac Low, 1995; Garcia-Segura et al., 1996; Walder & Folini, 1996) and many of its aspects were studied, the electron thermal conduction has not been considered yet in gasdynamical simulations. Since this energy transport mechanism may have an important impact on the WBB physics a numerical model which correctly treats its effects is the aim of this work. The gas dynamic model is described in Section 2. Section 3 presents the numerical model used in this study. The results are given in Section 4 and we discuss them in Section 5.

2. Gas dynamical model

Let us assume that at some initial time $t = 0$ a stellar wind (SW) with parameters $(\dot{M}_{\text{SW}}, V_{\text{SW}}, \mu_{\text{SW}}, \bar{\mu}_{\text{SW}}, M_0)$ starts blowing from the stellar surface R_0 onto the ambient uniform interstellar medium (ISM) with parameters $(n_{\text{ISM}}, T_{\text{ISM}}, \mu_{\text{ISM}}, \bar{\mu}_{\text{ISM}})$ where

$M_0 \gg 1$ is the Mach number at R_0 , μ – the mean weight per particle, $\bar{\mu}$ – the mean weight per nucleon, n_{ISM} and T_{ISM} are the ISM number density and temperature, respectively. For the typical values of the SW and ISM parameters the resulting flow is characterized by existence of two shocks and a contact discontinuity (Fig. 1). Because of the large typical values of V_{SW} , the gas in the interaction region II+III (Fig. 1) will have a very high temperature, the shock-heated plasma will be optically thin and its emission is expected to be mainly in the X-ray spectral domain. Besides, due to the existence of a high temperature in the interaction region and high temperature gradients in the vicinity of the shocks, remarkable influence of the electron thermal conduction on the flow is expected.

Thus, in the present study we consider 1D spherically symmetric flow with self-consistently taking into account the effects of the optically-thin-plasma

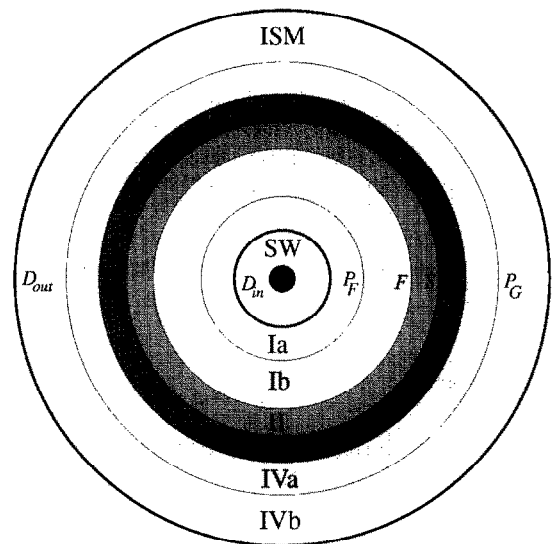


Fig. 1. A schematic diagram of the interaction between the stellar wind (SW) and the interstellar medium (ISM). F , G denote the two shocks, S – contact discontinuity, $P_{F,G}$ – the boundaries of preheating zones, $D_{in,out}$ – the boundaries of the calculation region. Regions I_a and IV_b are occupied by the undisturbed SW and ISM, respectively, regions I_b and IV_a – by the preheated SW and ISM, respectively, regions II and III – by the shocked SW and ISM, respectively.

cooling and the thermal conduction. For the case of such a flow the hydrodynamic equations read:

$$\begin{aligned} \frac{\partial \rho}{\partial t} + \frac{1}{R^2} \frac{\partial \rho v R^2}{\partial R} &= 0 \\ \frac{\partial \rho v}{\partial t} + \frac{1}{R^2} \frac{\partial (\rho v^2 + p) R^2}{\partial R} &= \frac{2p}{R} \\ \frac{\partial e}{\partial t} + \frac{1}{R^2} \frac{\partial (e + p) R^2}{\partial R} &= -Q_{\text{ems}} + Q_{\text{thc}} \end{aligned} \quad (1)$$

where ρ , v and p are the gas density, velocity and pressure, respectively; $e = p/(\gamma - 1) + \rho v^2/2$ is the total energy per unit volume; $\gamma = 5/3$ is the adiabatic index. The right-hand side terms in the energy equation of the system (Eq. (1)) are:

$$Q_{\text{ems}} = n_e n_H \lambda(T) \quad (2)$$

$$Q_{\text{thc}} = \frac{1}{R^2} \frac{\partial}{\partial R} \left(\delta \frac{C \varepsilon(Z)}{Z} T^{5/2} \frac{\partial T}{\partial R} R^2 \right) \quad (3)$$

where

$$n_e = \frac{\bar{\mu} - \mu}{\mu \bar{\mu}} \frac{\rho}{m_p}, \quad n_H = X_H \frac{\rho}{\bar{\mu} m_p}, \quad T = \frac{\mu}{R_g} \frac{p}{\rho},$$

$$\mu = \begin{cases} \mu_{\text{SW}}, & R < S \\ \mu_{\text{ISM}}, & R > S \end{cases},$$

$$\bar{\mu} = \begin{cases} \bar{\mu}_{\text{SW}}, & R < S \\ \bar{\mu}_{\text{ISM}}, & R > S \end{cases},$$

$$X_H = \begin{cases} X_{\text{H,SW}}, & R < S \\ X_{\text{H,ISM}}, & R > S \end{cases},$$

R_g is the universal gas constant, n_H and n_e – the hydrogen and the electron number density, respectively, m_p – the proton mass, $C = 9 \times 10^{-7}$, X_H is the relative hydrogen number density, $Z = (\bar{\mu} - \mu)/\mu X_H$ is the mean ion charge, $\varepsilon(Z)$ is a function having the asymptotic values $\varepsilon(1) = 3.1616$, $\varepsilon(\infty) = 12.47$ (Braginskii, 1957), δ_{SW} and δ_{ISM} are dimensionless reduction factors ($0 < \delta_{\text{SW,ISM}} \leq 1$) which are introduced artificially in order to take into account the damping effect of the SW and ISM magnetic fields and plasma fluctuations (see Section 5.1.2).

To determine the function $\lambda(T)$ (cooling curve) we used the model of Raymond & Smith (1977) including free-free, two-photon and recombination continua and emission lines of the elements H, He, C, N, O, Ne, Mg, Si, S, Ar, Ca, Fe, Ni and the following approximation:

$$\lambda(T) = \begin{cases} 7 \times 10^{-27} T, & T_{\text{cut}} \leq T \leq 10^5 \\ 7 \times 10^{-19} T^{-0.6}, & 10^5 \leq T \leq 4 \times 10^7 \\ 3 \times 10^{-27} T^{0.5}, & T \geq 4 \times 10^7 \end{cases}$$

where T_{cut} is the ‘cutting’ temperature which is usually accepted to be equal to 10^4 (see also Section 5.2.2). When a different chemical composition is considered we assume that the temperature dependence of the cooling curve does not change and only the particle number density changes correspondingly. This simplification is done just for technical reasons and it should not change our results qualitatively (e.g., the thin-plasma-cooling is important only in that part of the WBB which is occupied by the gas with solar abundances – the ‘pure’ hydrogen case, see Section 4).

If we normalize all the linear sizes to R_0 (where R_0 is some given distance), all the velocities to the terminal wind velocity V_{SW} , and the densities and pressures to $\dot{M}_{\text{SW}}/4\pi VR_0^2$ and $\dot{M}_{\text{SW}} V_{\text{SW}}/4\pi R_0^2$, respectively, the system of governing equations will have the form (Eq. (1)) with terms

$$Q_{\text{ems}} = \begin{cases} Q_1 = \Gamma_1 \tilde{T} \tilde{\rho}^2, & T_{\text{cut}} \leq T \leq 10^5 \\ Q_2 = \Gamma_2 \tilde{T}^{-0.6} \tilde{\rho}^2, & 10^5 \leq T \leq 4 \times 10^7 \\ Q_3 = \Gamma_3 \tilde{T}^{0.5} \tilde{\rho}^2, & T \geq 4 \times 10^7 \end{cases} \quad (4)$$

and

$$Q_{\text{thc}} = \Gamma_{\text{thc}} \frac{1}{R^2} \frac{\partial}{\partial R} \left(\delta \frac{\varepsilon(Z)}{Z} \left(\frac{\mu}{\mu_{\text{SW}}} \tilde{T} \right)^{5/2} R^2 \frac{\partial}{\partial R} \left(\frac{\mu}{\mu_{\text{SW}}} \tilde{T} \right) \right) \quad (5)$$

where $\bar{T} = \bar{p}/\bar{\rho}$ is a dimensionless temperature, Γ_1 , Γ_2 , Γ_3 and Γ_{thc} are dimensionless coefficients:

$$\Gamma_1 = 1.53 \times 10^4 \frac{\bar{\mu} - \mu}{\bar{\mu}^2} X_Z \dot{M}_{(6)} V_{(8)}^{-2} R_{0(12)}^{-1}$$

$$\Gamma_2 = 0.179 \frac{\bar{\mu} - \mu}{\mu^{1.6} \bar{\mu}^2} X_Z \dot{M}_{(6)} V_{(8)}^{-5.2} R_{0(12)}^{-1}$$

$$\Gamma_3 = 0.598 \frac{\bar{\mu} - \mu}{\mu^{0.5} \bar{\mu}^2} X_Z \dot{M}_{(6)} V_{(8)}^{-3} R_{0(12)}^{-1}$$

$$\Gamma_{\text{thc}} = 0.386 \mu_{\text{sw}}^{3.5} \dot{M}_{(6)}^{-1} V_{(8)}^5 R_{0(12)}$$

with notations $\dot{M}_{(6)} = \dot{M}_{\text{sw}}/10^{-6} M_{\odot} \text{yr}^{-1}$, $V_{(8)} = V_{\text{sw}}/10^8 \text{cm s}^{-1}$ and $R_{0(12)} = R_0/10^{12} \text{cm}$.

To introduce the physical boundary conditions we note that since the thermal conductivity depends on temperature nonlinearly, the preheating zones have finite sizes (Zel'dovich & Raizer, 1967). Therefore, we can expect (at least if the influence of thermal conduction is not extremely strong) that the non-stationary interaction of the supersonic SW with the ISM is characterized by preheating zones I_b and IV_a separated from undisturbed flows by the surfaces P_F and P_G (Fig. 1). In the undisturbed regions I_a and IV_b the gas temperature is low and, therefore, we can describe the flow with the help of a steady-state solution of the system (Eq. (1)) with $\tilde{Q}_{\text{ems}} = \tilde{Q}_{\text{thc}} = 0$ (sign tilde over dimensionless parameters hereinafter is omitted):

$$\begin{aligned} \rho &= \frac{1}{vR^2} \\ p &= \frac{1}{\gamma M_0^2} \left(\frac{(\gamma - 1)M_0^2}{(\gamma - 1)M_0^2 + 2} \right)^{\frac{\gamma+1}{2}} \rho^\gamma \\ v^2 &= -\frac{2}{\gamma - 1} \frac{\gamma p}{\rho} + 1 \end{aligned} \quad (6)$$

for the region I_a and

$$\rho = 3.31 \times 10^{-11} R_{0(12)}^2 \dot{M}_{(6)}^{-1} V_{(8)} n_{\text{ISM}}$$

$$p = 5.5 \times 10^{-19} R_{0(12)}^2 \dot{M}_{(6)}^{-1} V_{(8)}^{-1} n_{\text{ISM}} T_{\text{ISM}}$$

$$v = 0 \quad (7)$$

for the region IV_b , respectively. Taking $D_{\text{in}} < P_F$ and $D_{\text{out}} > P_G$, we can use the relations (Eq. (6)) and (Eq. (7)) for determining the physical boundary conditions at $R = D_{\text{in}}$ and $R = D_{\text{out}}$, respectively.

3. Numerical method

3.1. The general structure of the scheme

In our calculations we use a *soft fitting* technique developed by Godunov et al. (1979) on the basis of the Godunov scheme (Godunov, 1959). The technique allows to combine the advantages of the Eulerian and the Lagrangian approaches and, coupled with the method of the physical process splitting (Yanenko, 1967), allows to easily take into account various physical processes such as thermal conduction (e.g. Zhukov et al., 1993)

The essence of the technique can be shortly described as follows. Let us suppose that the state of the flow is known at the moment $t = t^n$. This means that the gasdynamical parameters (pressure, velocity and density) are known in the region bounded by H_{in} and H_{out} . The boundaries H_{in} and H_{out} may be mobile and this is also true for some fitted discontinuities $H_1 = F$, $H_2 = S$, $H_3 = G$ inside the flow. The positions H^n and velocities D_H^n of all the boundaries and discontinuities are also known at $t = t^n$. The law of motion of each mobile line may be given beforehand or determined during the calculations. Therefore, the mesh used in the calculations changes from a given time step to the consecutive one following the position of moving boundaries and discontinuities and any time step in the calculations may be conditionally divided into the following three sub-steps.

At the first sub-step, the positions of the mobile lines at the moment $t = t^{n+1}$ are determined:

$$H^{n+1} = H^n + D_H^n \tau \quad (8)$$

where $\tau = t^{n+1} - t^n$.

The second sub-step consists of remeshing at $t =$

t^{n+1} accordingly to the new positions of the lines. The simplest way to do it is to assume that between various discontinuities the grid vertices have a uniform distribution, but we do not need to restrict ourselves to this assumption. Thus, the grid vertices distributions at $t=t^n$ and $t=t^{n+1}$ forms a time-spatial structure $C(i) \equiv (R_{i-1/2}^n, R_{i+1/2}^n, R_{i-1/2}^{n+1}, R_{i+1/2}^{n+1})$ in the (R, t) space, where i denotes the cell number.

Finally, at the third sub-step the new values of the gasdynamical parameters and D_H^{n+1} in each mesh cell are obtained at the moment $t=t^{n+1}$. To do this, one should integrate Eq. (1) over the volume $C(i)$:

$$(V_i^{n+1} \sigma_i^{n+1} - V_i^n \sigma_i^n) / \tau = -(\Omega_{i-1/2} + \Omega_{i+1/2}) + (f_i^{(g)} + f_i^{(q)}) V_i^{n+1/2}$$

$$\sigma = (\rho, \rho u, e),$$

$$f^{(g)} = (0, 2p/R, 0), \quad f^{(q)} = (0, 0, -Q_{\text{ems}}),$$

$$\Omega = \Omega^{(g)} + \Omega^{(\text{thc})},$$

$$\Omega^{(g)} = (\Omega^\rho, \Omega^{\rho u}, \Omega^{(g)}), \quad \Omega^{(\text{thc})} = (0, 0, \Omega^{(\text{thc})}),$$

$$V = (R_{i+1/2}^2 - R_{i-1/2}^2) / 2, \quad (9)$$

where Ω^ρ , $\Omega^{\rho u}$, $\Omega^{(g)}$ and $\Omega^{(\text{thc})}$ are the mass, impulse, full enthalpy and thermal fluxes through the cell interface per unit time.

Following Zhukov et al. (1993) we substitute the system of equations (Eq. (9)) by the equivalent one

$$(V_i^{n+1} \sigma_i^{(g)} - V_i^n \sigma_i^n) / \tau = -(\Omega_{i-1/2}^{(g)} + \Omega_{i+1/2}^{(g)}) + f_i^{(g)} V_i^{n+1/2}$$

$$V_i^{n+1} (\sigma_i^{(q)} - \sigma_i^{(g)}) / \tau = f_i^{(q)} V_i^{n+1/2}$$

$$V_i^{n+1} (\sigma_i^{n+1} - \sigma_i^{(q)}) / \tau = -(\Omega_{i-1/2}^{(\text{thc})} + \Omega_{i+1/2}^{(\text{thc})}) \quad (10)$$

where $\sigma^{(g)}$ and $\sigma^{(q)}$ are defined below. This way of solving Eq. (9) is the finite-difference analogue of the physical processes splitting method which allows to take into account different physical processes independently by making use of various powerful

tools developed for studying the influence of each process.

3.2. The Godunov soft fitting scheme for adiabatic flows

Let us consider the first equation of the system (Eq. (10)) with

$$\sigma^{(g)} = (\rho^{n+1}, \rho v^{n+1}, e^{(g)})$$

To apply the Godunov (1959) scheme we write the fluxes $\Omega^{(g)}$ in the form:

$$\Omega_{i+1/2}^\rho = R_{i+1/2}^2 [\rho(U - W)]_{i+1/2}$$

$$\Omega_{i+1/2}^{\rho u} = R_{i+1/2}^2 [\rho(U - W)U + P]_{i+1/2}$$

$$\Omega_{i+1/2}^{(g)} = R_{i+1/2}^2 [E(U - W) + PU]_{i+1/2} \quad (11)$$

where $W = (R_{i+1/2}^{n+1} - R_{i+1/2}^n) / \tau$ is the edge velocity, ρ , U , P , E are respectively the density, velocity, pressure and total energy per unit volume at $t=t^{n+1/2}$ (which, following Godunov et al. (1979), we call *large* variables). The *large* variables and the moving discontinuities velocities D_H^{n+1} are determined from the exact solution of the local adiabatic Riemann problem with the piecewise-constant initial conditions at cells interfaces. Namely, the solution represents one of the the five possible configurations appearing when an arbitrary discontinuity decays, say, two shocks and contact discontinuity which velocities $\xi_1 < \xi_2 < \xi_3$ are known. Since W is also known one can determine the *large* variables as corresponding to the region bounded by ξ_k and ξ_{k+1} where k is determined from the condition $\xi_k < W < \xi_{k+1}$. Then, if the cell interface corresponds to the fitted discontinuities F , S , G or to the mobile boundaries $H_{\text{in, out}}$, the appropriate choice between ξ_k allows to determine D_H^{n+1} . For example, $D_S^{n+1} = \xi_2$ in the case when the cell interface corresponds to S . This way of determination of the discontinuity velocity allows just to mark the discontinuity instead of fitting it in the strict sense of the word. However, since it turns out that as a result of the described above mesh motion the discontinuities are spread out

over zero-one mesh points we call this procedure *soft fitting* technique.

The original Godunov scheme, assuming the piecewise-constant distribution of gasdynamic parameters inside the cell, is of the first order accuracy in space and time. To increase the resolution properties of the scheme, we introduce a piecewise-linear distribution of gasdynamic parameters inside each cell and apply some additional procedure to avoid oscillations of the solution around discontinuities (e.g., Sawada et al., 1989).

3.3. The scheme for cooling

Let us now consider the second equation of the system (Eq. (10)) with

$$\sigma^{(q)} = (\rho^{n+1}, \rho v^{n+1}, e^{(q)})$$

which, using Eq. (4), we rewrite in the form

$$\frac{V^{n+1} \rho^{n+1} (T^{(q)} - T^{(g)})}{(\gamma - 1)\tau} = -\Gamma_k T^{(q)\alpha_k} \rho^{n+1} V^{n+1/2} \quad (12)$$

where $\alpha_k = 1, -0.6, 0.5$ for $k = 1, 2, 3$, respectively, and the intermediate temperatures $T^{(q)}$ and $T^{(g)}$ are determined with the help of the following relations:

$$e^{(q,g)} = \rho^{n+1} (T^{(q,g)} / (\gamma - 1) + v^{n+1/2} / 2)$$

Performing the integration of Eq. (12) one can obtain:

$$T^{(q)} = \begin{cases} T^{(g)} \left(1 - \chi_k \tau \Gamma_k (\gamma - 1) \rho^{n+1} T^{(g)-\chi_k} \frac{V^{n+1/2}}{V^{n+1}} \right)^{1/\chi_k}, & \chi_k \neq 0 \\ T^{(g)} \exp \left(-\tau \Gamma_k (\gamma - 1) \rho^{n+1} \frac{V^{n+1/2}}{V^{n+1}} \right), & \chi_k = 0 \end{cases} \quad (13)$$

where $\chi_k = 1 - \alpha_k$. The first equation of Eq. (13) gives also the restriction on the time step (the temperature is a positive quantity) which should be coupled with the CFL condition when solving the system (Eq. (10)).

3.4. The scheme for thermal conduction

To describe the way we solve the third equation of the system (Eq. (10)) let us rewrite it in the form:

$$\frac{V^{n+1} \rho^{n+1} (T^{n+1} - T^{(q)})}{(\gamma - 1)\tau} = -(\Omega_{i-1/2}^{(\text{thc})} + \Omega_{i+1/2}^{(\text{thc})}) \quad (14)$$

where the thermal flux $\Omega^{(\text{thc})}$ can be determined with the help of Eq. (3) by introducing some fictitious dimensionless temperatures T^- , T^+ and fluxes $\Omega^{(\text{thc})-}$, $\Omega^{(\text{thc})+}$ at the corresponding cell interface (e.g. Fedorenko, 1994):

$$\Omega_{i+1/2}^{(\text{thc})-} = -\Gamma_{\text{thc}} \kappa_i (\mu_i^0 T^-)^{5/2} \frac{\mu_i^0 T^- - \mu_i^0 T_i}{R_{i+1/2} - R_i} R_{i+1/2}^2$$

$$\Omega_{i+1/2}^{(\text{thc})+} = -\Gamma_{\text{thc}} \kappa_{i+1} (\mu_{i+1}^0 T^+)^{5/2} \times \frac{\mu_{i+1}^0 T_{i+1} - \mu_{i+1}^0 T^+}{R_{i+1} - R_{i+1/2}} R_{i+1/2}^2$$

where $\kappa = \delta\varepsilon(Z)/Z$ and $\mu^0 = \mu/\mu_{\text{sw}}$. Using the conditions

$$\begin{aligned} \mu_i^0 T^- &= \mu_{i+1}^0 T^+ \equiv \mu_{i+1/2}^0 T_{i+1/2}, & \Omega_{i+1/2}^{(\text{thc})-} \\ &= \Omega_{i+1/2}^{(\text{thc})+} \equiv \Omega_{i+1/2}^{(\text{thc})} \end{aligned}$$

one can finally obtain

$$\Omega_{i+1/2}^{(\text{thc})} = -\Gamma_{\text{thc}} (\mu_{i+1/2}^0 T_{i+1/2})^{5/2} \times \frac{\kappa_i \kappa_{i+1} (\mu_{i+1}^0 T_{i+1} - \mu_i^0 T_i) R_{i+1/2}^2}{\kappa_i (R_{i+1} - R_{i+1/2}) + \kappa_{i+1} (R_{i+1/2} - R_i)} \quad (15)$$

with

$$\begin{aligned} &\mu_{i+1/2}^0 T_{i+1/2} \\ &= \frac{\mu_i^0 T_i \kappa_i (R_{i+1} - R_{i+1/2}) + \mu_{i+1}^0 T_{i+1} \kappa_{i+1} (R_{i+1/2} - R_i)}{\kappa_i (R_{i+1} - R_{i+1/2}) + \kappa_{i+1} (R_{i+1/2} - R_i)} \end{aligned} \quad (16)$$

Thus, Eqs. (14)–(16) can be written in a three-diagonal form:

$$\begin{aligned}
 & -P_{i+1/2}\mu_{i+1}^0 T_{i+1}^\nu + (s_i + P_{i-1/2} + P_{i+1/2})\mu_i^0 T_i^\nu \\
 & - P_{i-1/2}\mu_{i-1}^0 T_{i-1}^\nu = s_i T^{(q)} \\
 P_{i+1/2} &= \frac{\Gamma_{\text{thc}} \kappa_i \kappa_{i+1} (\mu_{i+1/2}^0 \hat{T}_{i+1/2})^{5/2} R_{i+1/2}^2}{\kappa_i (R_{i+1} - R_{i+1/2}) + \kappa_{i+1} (R_{i+1/2} - R_i)} \\
 s_i &= \frac{V_i^{n+1} \rho_i^{n+1}}{(\gamma - 1)\tau} \\
 \hat{T} &= \frac{1}{2}(T^{(q)} + T^{\nu-1}), \quad \nu = 1, \dots, Q, \\
 T^0 &= T^{(q)}, \quad T^{n+1} = T^Q
 \end{aligned} \tag{17}$$

where ν is an iteration number and Q is determined from the condition

$$\max_i |T_i^Q - T_i^{Q-1}| / T_i^{Q-1} < \epsilon \ll 1$$

On each iteration the system (Eq. (17)) is solved using Thomas algorithm (e.g. Hirsch, 1990) which we have tested with the help of exact solutions of the initial boundary-value problems for the nonlinear diffusion equation (Samarskii & Sobol, 1963).

4. Results

In order to study various effects of the physical processes included in the model, we consider a so called ‘standard’ wind-blown bubble (SWBB). It is assumed that it is a typical representative of the objects around luminous stars in the Galaxy. The SWBB is a result of interaction of the stellar wind from a star having parameters: $\dot{M}_{\text{SW}} = 1 \times 10^{-6} M_\odot$ and $V_{\text{SW}} = 2000 \text{ km s}^{-1}$ with the uniform interstellar matter with a number density of $n_{\text{ISM}} = 1 \text{ cm}^{-3}$. The interstellar/circumstellar matter is ionized by the radiation of the star and has a constant temperature of 12 000 K. For a technical consistency between different cases, we use the same grid, namely, having 50, 40, 80 and 20 grid points in regions I, II, III and IV, respectively. All the discontinuities (the contact one and the two shocks) are treated by the described above *soft fitting* technique which also allows to treat

properly different chemical compositions. Thus, the SWBB is such that the chemical composition of the SW is typical for the WR stars (that is ‘pure’ helium) while the ISM has solar abundances (‘pure’ hydrogen). The dependence of the solution on the mach number M_0 is not studied here because as it was shown by Myasnikov (1996) this parameter influences the solution only in the early stages of the evolution which are not interesting from an observational point of view. We kept therefore $M_0 = 50$.

In the next subsections we pay attention to the effects of the electron thermal conduction but for comparison the effects of the radiative cooling are considered as well.

4.1. Radiative cooling

Here we consider a radiative SWBB, that is, the radiative energy losses by an optically-thin plasma are self-consistently included in the model. As first was noted by Falle (1975), the radiative losses become very important at a certain moment of the bubble evolution and the outer shell (shocked interstellar gas) collapses. As a result, a secondary shock is formed which propagates towards the inner shock. This is well seen in Fig. 2 where the pressure, density and velocity profiles for the time interval between 6000 and 12 000 yr of the bubble evolution are shown. The pressure profile (Fig. 2a) is shown only in vicinity of the outer shock. This is so in order the formation of the pressure impulse due to the outer shell collapse to be better seen. Since the density values cover quite a big range of magnitudes, the density profiles (Fig. 2b) are shown separately for the inner and the outer part of the SWBB. The position of the contact discontinuity coincides with the big density gradient splitting the bubble in two parts: inner one (low density) and outer one (high density).

For the chosen set of physical parameters, which basically determine the wind-interstellar-matter interaction, the cooling in the outer shell becomes very important at the bubble age of about 6000 yr which is followed by a collapse of the outer shell; a

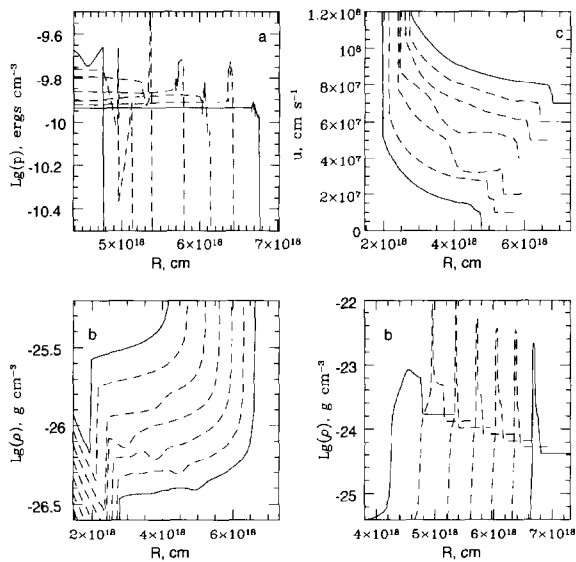


Fig. 2. The pressure (a), density (b) and velocity (c) profiles in the case of a purely radiative SWBB during the bubble evolution between 6000 and 12 000 yr with a time step of 1000 yr. The solid lines denote the two limited time cases. For clarity, the density profiles are shifted by -0.1 dex each with respect to the previous one while the velocity ones – by 10^7 cm s^{-1} (the difference between the 8000 and 9000 yr profiles is two times bigger)

pressure impulse is formed (Fig. 2a) and secondary shocks form. As noted by Falle (1975), one of the secondary shocks moves towards the outer shock, and their interaction can be noted by the irregular changing of the pressure near the outer shock, while the other wave penetrates in the opposite direction. The large length scale in the bubble interior allows us to follow its evolution. After the reflection of the secondary shock from the inner shock (between 9000 and 10 000 yr of the bubble age), the intensity of the former gradually decreases and at a later stage of the bubble evolution no secondary shocks are ever formed. This might well be related to the fact that at later stages of the bubble evolution the temperature of the outer shell is always below 10^5 K which means that only the last branch ($Q \propto T$) of the cooling curve is important and this prevent the further fast collapse of the shell.

4.2. Thermal conduction

The case of purely conductive SWBB is, of course, only of academic interest but it is worthwhile to consider it since these results can be used to reveal the effects of different physical processes. Fig. 3 shows the SWBB for the interval of its evolution between 6000 and 12 000 yr. The pressure profile (Fig. 3a) is shown in vicinity of the outer shock in order to have a better comparison with the radiative SWBB.

The difference with the radiative case is immediately seen. First, while in the radiative case the inner shock is adiabatic (the energy losses are not important in the hot bubble due to its low number density) it has now become isothermal because of the large thermal flux from the hot bubble to the free wind. The isothermity of the inner shock is well denoted by the large density jump which perfectly corresponds to the theoretical value of M^2 (where M is the Mach number) for the isothermal shock. Second, the effect of different chemical compositions of the stellar wind and the interstellar medium is also well demonstrated by the density jump at the contact discontinuity. We would like to stress that this was possible to be found only because of the use of the *soft fitting* technique. On the other hand, this density jump is well understood since the thermal conduction equals the temperature on both sides of the contact discontinuity, the pressures are equal as well and as a result the number densities must be also equal. This results in different densities and the density ratio must be equal to the ratio of the mean atomic weights per particle. In our case of ‘pure helium’ wind and a ‘pure hydrogen’ interstellar gas this ratio is 1.3 : 0.5 which is exactly what is seen in Fig. 3b. Third, there are no waves formed in the purely conductive SWBB since the thermal conduction only redistributes the internal energy between the different parts of the bubble and there are no real energy sinks.

Fig. 3 also demonstrates the so called cold shell ‘evaporation’ which is well seen in the density profiles (Fig. 3b). First we see that the outer shock is quasi-adiabatic (a density jump of about 4) since the

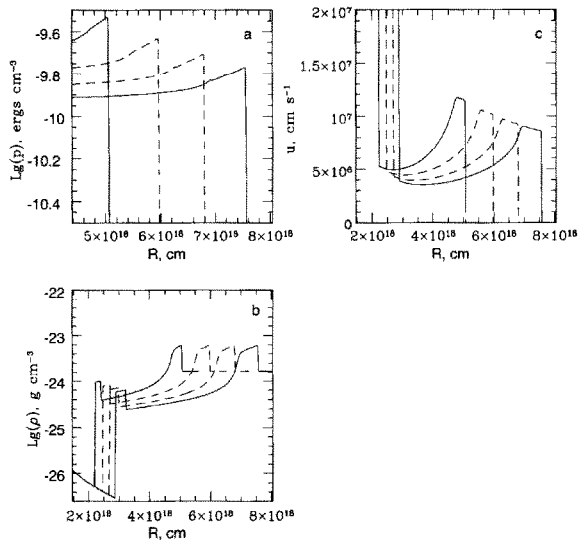


Fig. 3. The pressure (a), density (b) and velocity (c) profiles in the case of a purely conductive SWBB during the bubble evolution between 6000 and 12 000 yr with a time step of 2000 yr. The solid lines denote the two limited time cases.

shock velocity is not very high which results in a smaller temperature jump and a small electron conduction efficiency as well. Since there are no energy losses (cooling) the outer shell is much thicker than it is at the same age of the radiative SWBB evolution (see Fig. 2b). Another important difference is that the density decreases gradually into the bubble interior and the hot bubble is much denser with respect to the radiative case (note the y-axis scales in Fig. 2b and Fig. 3b). This behaviour can be understood as follows. Due to the thermal conduction flux from the hot bubble, the outer (cold) shell is heated and as a result its gas temperature increases. Its gas pressure increases as well until a new pressure balance with the hot bubble is reached. Since the hot bubble loses internal energy and the cold shell gains it, the size of the former decreases and the size of the latter increases and this is the cold shell ‘evaporation’. Thus, the electron conduction influence results in a much denser and with a lower temperature interior of the SWBB with respect of the radiative case and the mass of the hot bubble is

dominated by the ‘evaporated’ mass from the cold shell.

4.3. Cooling and thermal conduction

In the previous two subsections we considered, respectively, the net effects of the thin-plasma cooling and thermal conduction on the physics of the WBB. A more realistic model of the wind-interstellar-matter interaction will then be if their simultaneous effects are taken into account. Fig. 4 presents the result of the SWBB modelling in the time interval from 6000 to 20 000 yr of the bubble evolution. All previously mentioned major features are also seen here. Namely, the collapse of the outer shell and the secondary shock formation, the effect of different chemical composition, the isothermity of the inner shock. It should be noted that the big density gradient, seen in vicinity of the outer (collapsed) shell, does not indicate the contact discontinuity. It is a result of the cold-shell ‘evaporation’ and the density-profile steepness reflects the strong temperature dependence of the electron thermal conduction. The position of the contact discontinuity is found by the density jump near the inner shock. On the other hand, there is a big difference between the case under consideration and the cases of purely radiative and purely conductive WBB, that is the existence of wave(s) bouncing forth and back between the outer and the inner shocks during the whole bubble evolution after the outer shell has collapsed. This is well seen in the profiles of all physical quantities but it is better demonstrated in the velocity profile. In fact, we can easily note a wave (it is probably a shock formed by the outer shell collapse) propagating towards the inner shock at the bubble age of 10 000–14 000 yr. After its reflection from the inner shock this wave is moving back to the outer shock and at an age of about 16 000 yr it interacts with the newly formed wave propagating again towards the inner shock. These multiple waves interaction (we will denote this phenomenon as multiple shock waves, MSW, throughout this paper) can be readily followed during the bubble evolution.

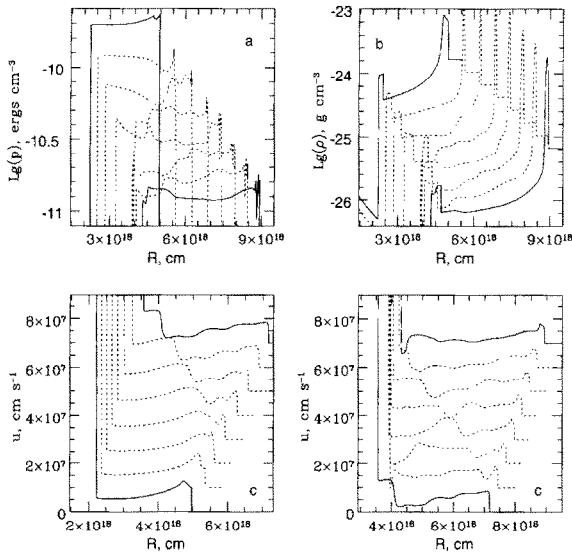


Fig. 4. The pressure (a), density (b) and velocity (c) profiles in the case of the SWBB (cooling and conductivity considered) during the bubble evolution between 6000 and 20 000 yr with a time step of 2000 yr for (a) and (b) and of 1000 yr for (c). The solid lines denote the two limited time cases. For clarity, the pressure profiles are shifted by -0.1 dex each with respect to the previous one, the density profiles – by -0.2 dex and the velocity ones – by 10^7 cm s^{-1} (the 13 000 yr profile is shown twice, first, in the left panel – up, and then in the right panel – down).

Of course, it is natural to ask whether these waves are physical or numerical and we will additionally address this item below. On the other hand, some conclusions, supporting their physical nature, could be drawn in a straightforward way from the previous cases. Namely, we do not see any waves in the purely conductive WBB while we do see a secondary wave/shock (we will name this wave a ‘Falle wave’, FW, throughout the text) in the purely radiative case. So, if we assume that the FW is real, we can propose the following mechanism for the MSW formation. In general, the hot bubble is an ‘container’ of energy which, thanks to the thermal conduction, is permanently spread over the whole bubble volume. This means that a thermal wave is continuously propagating into the cold shell and heats it up. On the other hand, the cold-shell density is already such that the radiative cooling is very important and the supplied

energy is permanently lost by emission. Each of this mechanisms has its own characteristic timescale and their combined effect acts as an energy ‘pump’. First, the outer-shell gas is ‘instantaneously’ heated up (because of the physical nature of the thermal conduction) and the additional energy is emitted later on due to the cooling. This can also explain why there are no FWs in the late stage of purely radiative bubble, namely, because there is no additional energy supply to the cold shell.

5. Discussion

The 1-D results on the SWBB with taking into account the electron thermal conduction can serve as a basis for our understanding of these objects. They can be further developed to be closer to the reality by considering the two-dimensional effects. Before doing such a consideration, it is our impression, that a question of a fundamental importance is that about the reality of the waves (FW and MSW) found in the numerical simulations. This is so since if these waves are physical then they can cause some instability developments when the two-dimensional effects are being considered.

5.1. Comparison with the similarity solution

To check our calculations we compared the numerical results with the self-similar solutions obtained by Weaver et al. (1977).

5.1.1. Adiabatic WBB

We have started with the comparison between our numerical solution and the similarity one, given by Weaver et al. (1977) for the case of an adiabatic WBB. As described by these authors, the structure of the WBB can be derived separately for the inner (shocked stellar wind gas) and the outer (shocked interstellar gas) parts. To do that, we followed the procedure, given by Weaver et al. (1977), in the case of the SWBB. Fig. 5a–c shows the density, pressure and velocity profiles for the SWBB at its age of 10 000 yr. It is seen that the numerically found

profiles perfectly coincide with those given by the similarity solution. More precisely, the differences between the similarity solution and the hydrodynamic computations are less than 1% for the position of the outer shock and less than 3% for the position of the inner. An accuracy of better than 1% is also found for the position of the contact discontinuity. When plotting the pressure profile, we corrected its value given by the similarity solution by a factor of $[G_{\text{sim}}/G_{\text{num}}]^3$. Thus we can prove that, on the one hand, the assumptions behind the similarity solution are consistent with the WBB physics and, on the other hand, our numerical technique is able to handle properly the time-dependent flows with strong shocks.

5.1.2. Conductive WBB

Our numerical results can be also compared with the similarity solution found by Weaver et al. (1977) for the thermal conductive case. Weaver et al. have assumed that the thermal conduction is the main energy transport mechanism governing the interior of

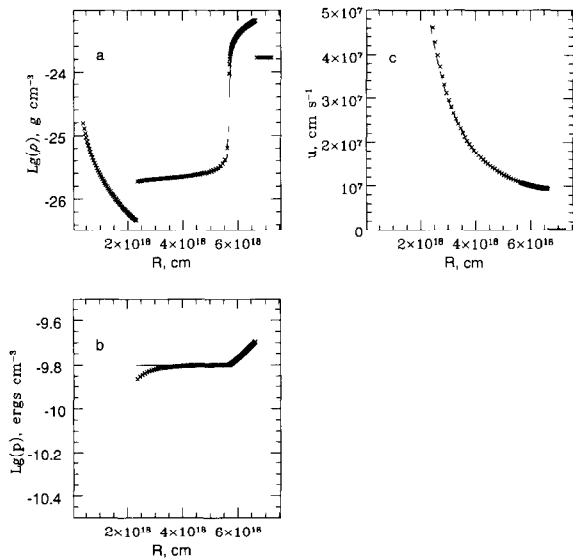


Fig. 5. A comparison of the density, pressure and velocity profiles between the numerical hydrodynamic calculations (dots) and the similarity solution (solid lines) for the case of the adiabatic SWBB at its evolution age of 10 000 yr.

the WBB and considered its late stage after the outer shell has collapsed. Fig. 6a–d shows the temperature, density, pressure and velocity profiles for the SWBB case at its age of 10 000 yr where the solid line denotes the Weaver et al. solution (derived by solving Eqs. (30) and (31) given in their paper) while the points correspond to the numerical hydrodynamic results. It is seen that the correspondence between the two types of solution is very good for all the quantities but the velocity. Having in mind the MSW (see above), the last is not a surprise since the similarity technique is not capable of treating such phenomena. We would like to note that the profiles derived from the similarity solution are shown only to the inner edge of the hot bubble (the inner shock) since this solution gives no indication on the position of that hot-bubble border. Also, we would like to mention that the similarity solution gives a slightly wrong position (less than 10%) of the outer radius (the outer shock) of the WBB (a correction for this has been made while presenting the results in Fig. 6a–d). This result is understandable since it is not possible to follow the complete WBB evolution when applying this technique. For example, in this case, first, we are not able to self-consistently consider the collapse of the outer shell and instead the WBB evolution is split in two parts: before and after the cold-shell collapse, respectively. Second, the similarity solution cannot handle the change in the physical conditions of the interstellar gas due to the thermal conduction (there exists a preheating zone in the early stages of the WBB evolution while the cold-shell temperature is still high enough, that is before the shell collapse).

Also, it is worth noting some limitations of the similarity solution by Weaver et al. (1977). This solution is physically incomplete since the cooling is not self-consistently included in the WBB physics. While this is not important for the hot-bubble interior (due to its low density), the radiative losses play important role in the transition zone between the cold shell and the hot bubble. Namely, this is the reason for the MSW appearance (see above). Additionally, Weaver et al. assume that the contact discontinuity and the outer shell coincide at a later stage of the

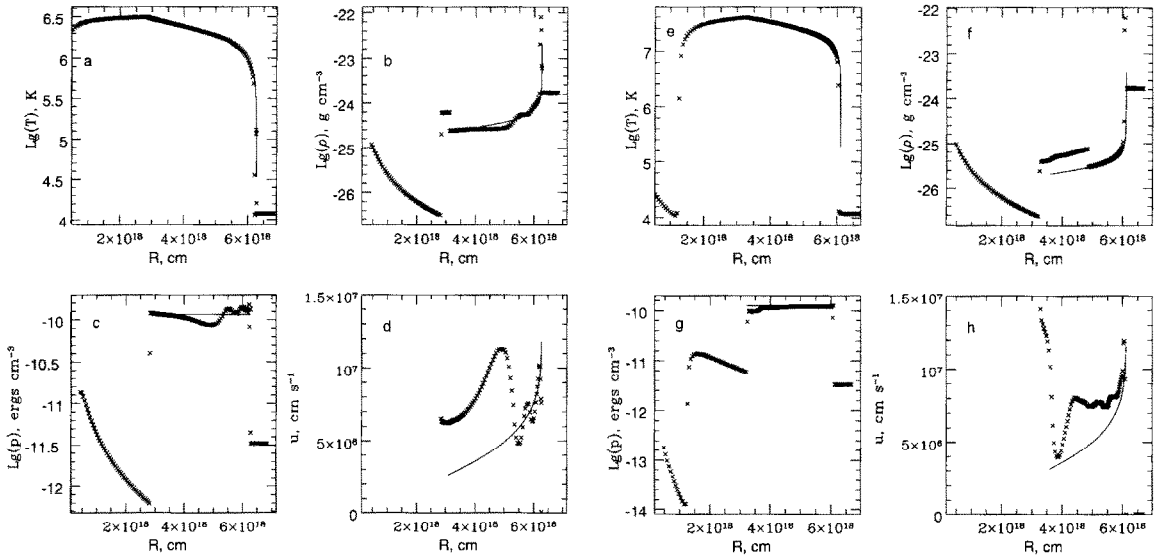


Fig. 6. A comparison of the temperature, density, pressure and velocity profiles between the numerical hydrodynamic calculations (dots) and the similarity solution (solid lines) for the case of the SWBB (thermal conductivity and cooling included) at its evolution age of 10000 yr. (a–d) present the standard case and (e–h) show the case with ‘reduced’ thermal conductivity.

bubble evolution, that is after the outer-shell collapse due to the rapid cooling. Instead, the hydrodynamic calculations show that the contact discontinuity has moved towards the inner shock (see the density jump near the inner shock in Fig. 3b, Fig. 4b and Fig. 6b) and the big density gradients in vicinity of the cold shell are result of the cold-gas ‘evaporation’. Nevertheless, it is our impression that the similarity solution gives a relatively well representation of the hot-bubble interior and it could be used for estimating some of its spectral characteristics.

5.1.3. ‘Reduced’ thermal conduction

An interesting case can be considered which is somehow intermediate between those considered above, namely, this is the case when the thermal conduction is suppressed due to some physical conditions (e.g., existence of magnetic fields, plasma fluctuations). In order to have an idea about the expected effects we consider the case when the thermal conductivity is simply reduced by some factor while its dependence on temperature remains the same. We would like to note that in the one-

dimensional case this is the only possibility to study such an effect.

For this purpose we use the introduced in Section 2 dimensionless coefficient δ which denotes the reduction factor for the thermal conductivity and it is thus less than unit ($\delta \leq 1$). In this case we can also consider a similarity solution for the hot bubble structure and its basic equations (Eqs. (30) and (31) in Weaver et al., 1977) will now read:

$$\frac{3}{2}U - \delta\tau^{5/2}\frac{d\tau}{d\xi} = \frac{2}{5}\xi + \frac{11}{10\xi^2} \quad (18)$$

$$\delta\frac{\tau}{\xi^2}\frac{d}{d\xi}\left(\xi^2\tau^{3/2}\frac{d\tau}{d\xi}\right) - \frac{11}{10}\frac{1-\xi^3}{\xi^2}\frac{1}{\tau}\frac{d\tau}{d\xi} = \frac{13}{35} \quad (19)$$

These equations can be solved in order to derive a similarity solution which then can be compared with the exact hydrodynamical one. We note that if $\delta = 1$ one gets the corresponding equations given by Weaver et al. Fig. 6e–h shows the structure of the SWBB when the thermal conductivity was reduced by a factor of 10^4 , thus, $\delta = 10^{-4}$. As in Fig. 6a–d,

the solid line denotes the similarity solution (from Eqs. (18) and (19)) and the dots present the exact hydrodynamic results (as mentioned above, the similarity solution profiles have been corrected for the deviation of the outer shock position from its exact value). It is seen that the hot-bubble gas temperature is higher in this case which is well understood since a smaller part of its internal energy has been supplied into the cold shell. This also explains why the density profile shows a larger extension of that part of the hot bubble, occupied by the shocked wind gas, and a smaller size of that part consisting of gas ‘evaporated’ from the cold shell. This, with the smaller preheating zone in the free-blown wind (Fig. 6a,c and Fig. 6e,g), is a natural result from the thermal conduction being less efficient. On the other hand, the ‘reduced’ thermal conduction flux is still big enough to cause formation of the MSW which are well demonstrated by the velocity profile (Fig. 6h).

5.2. Are the numerically found waves real?

5.2.1. Soft fitting vs. capturing

In order to confront the *soft fitting* technique with the ‘traditional’ *capturing* one we run the same case of the SWBB using a fixed grid with $H_{in} = 2R_0$, $H_{out} = 65R_0$ and 2000 grid points. The velocity profiles at the bubble age of $t = 6000, 8000, 10\,000, 12\,000, 16\,000, 18\,000, 20\,000$ yr are presented in Fig. 7a.

One can see that the FW is generated only once unlike the case presented in Fig. 4 (*soft fitting*) but small-scale oscillations are seen around the inner shock. These oscillations have a numerical origin indeed because we do not see them when using the *soft fitting* technique which, as our experiments show, allows to obtain nonoscillating solution in the vicinity of a *soft-fitted* shock even without any additional slope limiting procedures. Thus, no MSW are found in the case of the fixed grid. It is suggestive that this discrepancy may be a result of that the outer shock is numerically worse described (captured) in the case of the fixed grid. Really, the outer shock on the later stages of the bubble evolu-

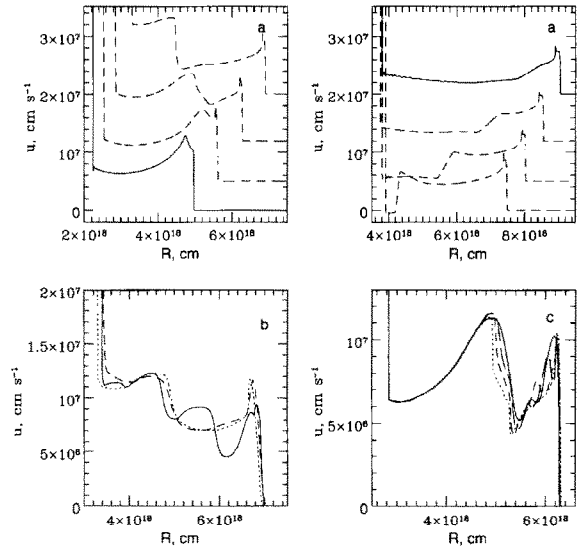


Fig. 7. Multiple shock waves at different grid characteristics. (a) – the velocity profiles in the SWBB during the bubble evolution between 6000 and 20 000 yr with a time step of 2000 yr. The solid lines denote the two limited time cases. For clarity, the velocity profiles in the both panels are shifted by 5×10^7 cm s⁻¹, 7×10^7 cm s⁻¹ and 8×10^7 cm s⁻¹, respectively, each with respect to the previous one. A stationary fixed grid was used. (b) – the velocity profiles in the SWBB at its age of 12 000 yr in the cases of: stationary ($D/V = 0.0$) fixed grid (dots), fixed grid moving with a constant velocity $D/V = 0.05$ (solid line), and fixed grid moving with a constant velocity $D/V = 0.1$ (dashed line). (c) – the velocity profiles in the SWBB at its age of 10 000 yr with different number of grid points in the bubble interior: 80 – solid line; 160 – long dash; 320 – short dash; 640 – dots. The *soft fitting* technique was used.

tion when its intensity decreases due to the decrease of its velocity is spread on two-three grid points in the case of a fixed grid but on zero points when the *soft fitting* technique is applied. On the other hand, the MSW may be generated by the probable small errors in the realization of the more complicated *soft fitting* technique.

In order to check which one is the case, we carried out a set of calculations using the capturing technique but on moving mesh. Namely, we moved the whole calculation region with the velocities $D/V_{sw} = 0, 0.05, 0.1$ ($D_{H_{in}} = D_F = D_S = D_G = D_{H_{out}} = D/V_{sw}$), which also means that all the vertices of the

grid were moving with the same velocity. The choice $D/V_{\text{sw}} = 0.05$ corresponds approximately to the outer shock velocity at the moment $t = 10\,000$ yr when the cooling manifests itself by generating additional FWs. The results of the calculations performed with 200 grid points between H_{in} and H_{out} for the same case of the SWBB at its age of $t = 12\,000$ yr are presented in Fig. 7b. One can see that the additional FW appears only in the case with $D/V_{\text{sw}} = 0.05$. As far as the essence of the *soft fitting* technique is the moving of the grid with a velocity equal to the discontinuity velocities (Section 3), we can conclude that when the whole computational region is moving with $D/V_{\text{sw}} = 0.05$ we efficiently fit the outer shock in the same way as done by the *soft fitting* technique, and in this case the both techniques are equivalent. On the other hand, since all three considered cases ($D/V_{\text{sw}} = 0, 0.05, 0.1$) are equivalent from a technical point of view, we can conclude that the MSW are not caused by some numerical errors in the realization of the *soft fitting* technique and we do not see these waves on the fixed grid only because we are not able to resolve the outer shock well enough in order to study such fine scale behaviour of the solution. Also, we do see the primary FW on the fixed grid because it appears when the outer shock still has a high velocity and therefore intensity which allows to capture the shock better.

Another experiment we performed is to increase the resolution (the number of grid points) in region III where the MSW manifest themselves. We considered the SWBB and applied the *soft fitting* technique. The results at the bubble age of 10 000 yr are presented in Fig. 7c. One can see that the MSW have a qualitatively similar behaviour on different meshes, therefore, we can conclude that the reason of the MSW appearing is physical rather than numerical.

5.2.2. The influence of the cooling curve cutting

One of the main limitations in our model is that related to the thin-plasma cooling. It is assumed that the radiative cooling is important in the entire temperature range but below some ‘cutting’ temperature value. This means that the cooling is decoupled

from the radiation of the central star which is responsible for the ionization of the interstellar gas. The last is qualitatively reproduced by the cooling cut-off temperature since in such a way it is ensured that the gas cannot cool below this value, that is, an ionization equilibrium is established which is representative for the ionization nebulae with an almost constant gas temperature. On the other hand, such a treatment of the shock-heated-gas cooling and its interaction with the central star radiation may suffer some weakness since this means that down to the ‘cutting’ temperature value the cooling curve has some non-zero values and it ‘instantaneously’ makes a jump to zero just below this temperature. Moreover, since other, secondary, discontinuities have appeared during the WBB evolution (FW and MSW), it is of a great importance to study the influence of this discontinuous behaviour of the cooling curve on the secondary waves parameters.

In order to study the influence of the cooling curve

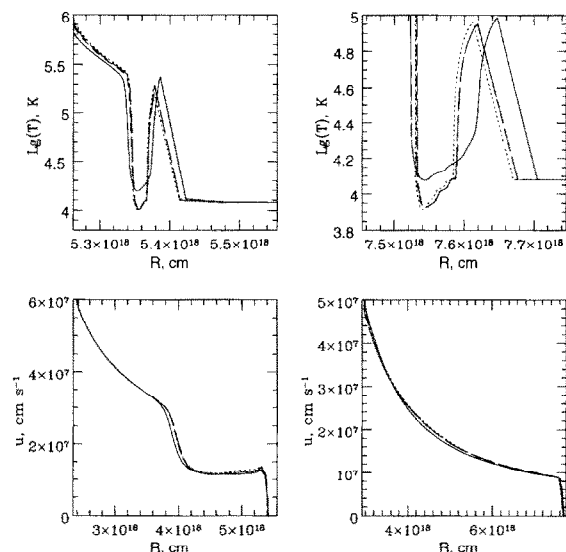


Fig. 8. The influence of different shape of the ‘cutting’ function in the cooling curve in the case of the purely radiative SWBB at its age of 8000 (left panels) and 15 000 yr (right panels), respectively. Lines: dotted – ‘jump’; short dash – linear; long dash – quadratic; solid – exponential (see the text).

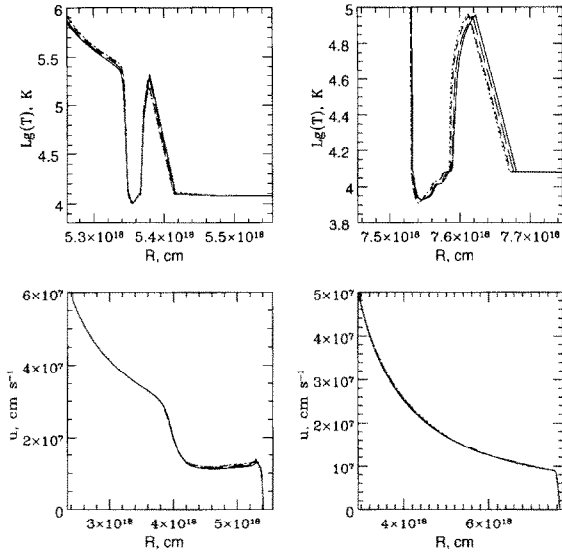


Fig. 9. The influence of different values of T_{cut} in the case of purely radiative SWBB at its age of 8000 (left panels) and 15000 yr (right panels), respectively. The shape of the ‘cutting’ part of the CC is linear and $T_{\text{zer}} = 12000$ K in all cases. Lines: dotted – $T_{\text{cut}} = 12000$ K; short dash – $T_{\text{cut}} = 15000$ K; long dash – $T_{\text{cut}} = 30000$ K; solid – $T_{\text{cut}} = 60000$ K.

($\lambda(T)$) cutting on the MSW evolution we have considered the following general cases:

- (1) the $\lambda(T)$ has its normal shape down to the ‘cutting’ temperature, T_{cut} , and it is equal to zero just below it;
- (2) the $\lambda(T)$ has its normal shape down to T_{cut} , and it linearly goes to zero between this temperature and T_{zer} ;
- (3) the $\lambda(T)$ has the same behaviour as in case (2) but it goes to zero quadratically;
- (4) the same as in case (2) and (3) but the $\lambda(T)$ goes to zero exponentially.

We would like to mention that case (2) was introduced with the aim to avoid the discontinuity in the $\lambda(T)$. Case (3) further guarantees that there is no discontinuity neither in the $\lambda(T)$ nor in its first derivate. Case (4) is considered to be closer to the

expected behaviour of the total radiative cooling if the photoionization has been also taken into account. Indeed, one can expect some quasi-exponential behaviour below some temperature where the photoionization becomes important since in this case all the processes (energy losses and gains) are roughly proportional to the mean gas temperature (which is in its turn related to the stellar photospheric temperature). It is worth noting that in this picture T_{zer} is representative of the equilibrium temperature of the interstellar/circumstellar gas.

Fig. 8 presents the results for the purely radiative SWBB (no thermal conduction) for the four cases listed above with the following $\lambda(T)$ parameters: (1) $T_{\text{zer}} = T_{\text{cut}} = 12000$ K; and for (2), (3) and (4) – $T_{\text{zer}} = 12000$ K and $T_{\text{cut}} = 30000$ K; The temperature and density profiles (which are of main astrophysical interest) are presented in the left panels for the bubble age of 8000 yr and the same is shown in the right panels of Fig. 8 for the age of 15000 yr. We consider in details only the outer part (between the contact discontinuity and the outer shock) of the SWBB since the cooling is important only there while the profiles of the all quantities coincide in the interior of the hot bubble independently on the different behaviour of the $\lambda(T)$. It is well seen that there are no big differences in the profiles of the physical parameters between the cases under consideration. Indeed, the actual differences (e.g., in the position of the outer shock etc.) are less than 1% (note the length scale in the figures).

Another important parameter which may influence the cold shell structure is T_{cut} . Fig. 9 shows the results for the purely radiative SWBB in the cases with $T_{\text{cut}} = 12000, 15000, 30000$ and 60000 K, respectively. In all the models T_{zer} was 12000 K and the behaviour of the $\lambda(T)$ between T_{cut} and T_{zer} was linear. The structure of Fig. 9 is the same as in Fig. 8 and the results show that no reasonable differences are seen between the different cases.

Additionally, we have considered the same cases as those shown in Figs. 8,9 but the thermal conduction was also taken into account. The results of these simulations are presented in Figs. 10,11, respectively. The only difference in these figures with the

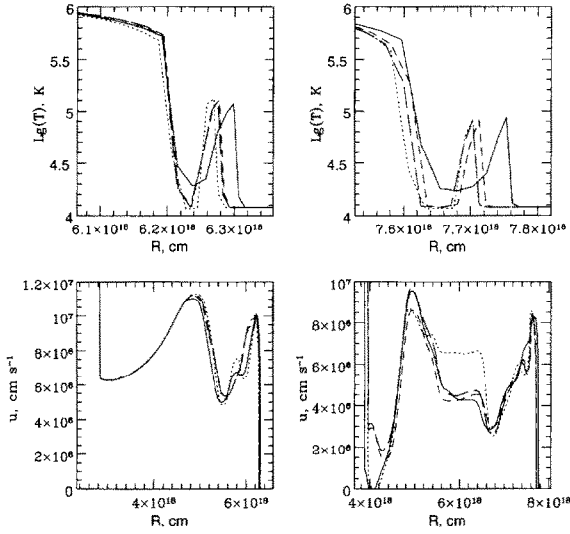


Fig. 10. The influence of different shape of the 'cutting' function in the cooling curve in the case of the SWBB (cooling and conductivity considered) at its age of 10 000 (left panels) and 15 000 yr (right panels), respectively. Lines: dotted – 'jumps'; short dash – linear; long dash – quadratic; solid – exponential (see the text).

previous two is that the left panels show the results for the bubble age of 10 000 yr. This was done since we are mainly interested to study the $\lambda(T)$ influence on the MSW which are well developed after about 8000–9000 yr of the SWBB evolution (see Fig. 4). Also, the velocity profile was chosen instead of that of the density since the MSW are better seen in the former. As in Figs. 8,9, the temperature profiles are shown in vicinity of the outer shell while the velocity profiles are shown in the region between the inner and the outer shocks. Figs. 10,11 show that the conclusion drawn for the purely radiative case is in general valid in this case too. On the other hand, we would like to mention that the gradient of the $\lambda(T)$ in its part where it goes to zero seems to play more important role here. For example, the velocity profile is more 'sensitive' to the existence of a discontinuity in the $\lambda(T)$ at later bubble age (see the right panels in Fig. 10) and the same is true when a higher gradient

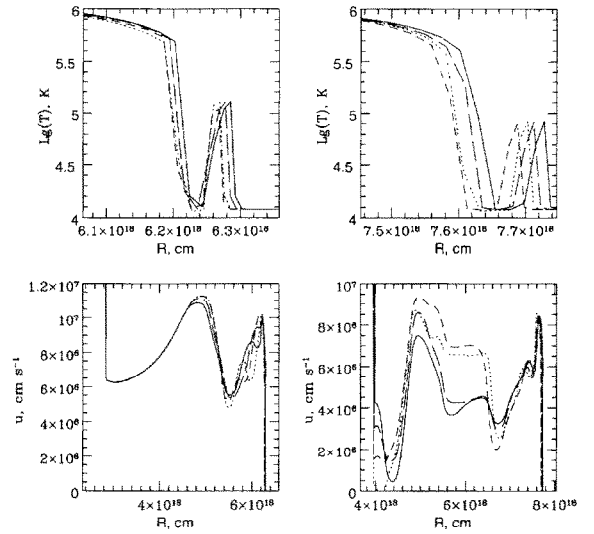


Fig. 11. The influence of different values of T_{cut} in the case of the SWBB (cooling and conductivity considered) at its age of 10 000 (left panels) and 15 000 yr (right panels), respectively. The shape of the 'cutting' part of the CC is linear and $T_{zer} = 12\,000$ K in all cases. Lines: dotted – $T_{cut} = 12\,000$ K; short dash – $T_{cut} = 15\,000$ K; long dash – $T_{cut} = 30\,000$ K; solid – $T_{cut} = 60\,000$ K.

exists in the $\lambda(T)$ (see the right panels in Fig. 11). In fact, the lower T_{cut} the steeper the $\lambda(T)$ goes to zero. However, a general conclusion is straightforward even in this case, namely, that the different shapes of the $\lambda(T)$ (see above) and different values of T_{cut} give qualitatively the same behaviour of the MSW.

Finally, the analysis of the results presented here makes us confident to draw a conclusion that the numerically found waves in the purely radiative case (FW) as well as in the physically more complete one with the thermal conduction considered (MSW) are physical rather than an artifact from our numerical code. Thus, the mechanism of continuous energy 'pumping' from the hot bubble into the cold shell with its consecutive emission due to the fast cooling may have an important impact on the WBB physics. Its two-dimensional consideration is definitely worthy since it may shed light on the formation of some irregular structures observed in these objects.

6. Conclusions

We have considered a numerical 1D model of wind-blown bubbles which self-consistently takes into account the optically-thin-plasma cooling and the electron thermal conductivity. The model is based on the use of the *soft fitting* technique. The main results of this study can be noted as follows.

- A comparison between the numerical solution and the existing self-similar one shows that the latter is accurate enough for all the physical quantities profiles but that of the gas velocity in the bubble interior. Thus, the similarity solution can be used for having estimates of some spectral characteristics of the hot bubble.
- At a given stage of the wind-blown-bubble evolution multiple shock waves appear. They are result of a combined effect of the plasma cooling and the electron thermal conduction. Various tests have been performed which made us confident that these waves have a physical nature rather than being an artifact of the numerical simulations. A two-dimensional model of the wind-blown bubbles is therefore quite welcome in order to study the influence of these waves on the stability properties of these objects.
- A comparison between the *soft fitting* technique and the more 'traditional' capturing one shows that the former is superior. For example, it better fits the shock discontinuities and gives the same spatial resolution by making use of a smaller number of grid points (the last means that it is less time consuming too).

Acknowledgements

This work was partially sponsored by the National Science Fund of the Bulgarian Ministry of Education, Science and Technologies under contract F-570. The authors also acknowledge the ESO C&EE Programme Travel Grant No. A-07-036.

References

- Bochkarev, N.G., 1988, *Natur*, 332, 518.
- Braginskii, S.I., 1957, *Zh. Theor. i Eksp. Phys.*, 33, 459.
- Brighenti, F. & D'Ercole, A.D., 1995a, *MNRAS*, 273, 443.
- Brighenti, F. & D'Ercole, A.D., 1995b, *MNRAS*, 277, 53.
- Brighenti, F. & D'Ercole, A.D., 1997, *MNRAS*, 285, 387.
- Chu, Y.-H., 1981, *ApJ*, 249, 195.
- Conti, P.S. & Underhill, A.B., 1988, *O stars and WR stars*, NASA SP-497.
- D'Ercole, A.D., 1992, *MNRAS*, 255, 572.
- Falle, S.A.E.G., 1975, *A&A*, 43, 323.
- Fedorenko, R.P., 1994, *Vvedenie v Vichislitel'nyu Fiziku*, Moscow Institute of Physics and Technology Publishers, Moscow.
- Garcia-Segura, G. & Mac Low, M.-M., 1995, *ApJ*, 455, 160.
- Garcia-Segura, G., Mac Low, M.-M., & Langer, N., 1996, *A&A*, 305, 229.
- Godunov, S.K., 1959, *Mat. Sbornik*, 47, 271.
- Godunov, S.K., Zhabrodine, A.V., Ivanov, M. Ya, Kraiko, A.N., & Prokopov, G.P., 1979, *Resolution Numerique des Problemes Multidimensionnels de la Dynamique des Gaz*, Editions MIR, Moscow.
- Hirsch, C., 1990, *Numerical Computation of Internal and External Flows*, John Wiley & Sons Ltd, New York.
- Lozinskaya, T.A., 1982, *Ap&SS*, 87, 313.
- Myasnikov, A.V., 1996, *Gasdynamic Modelling of Some Time Dependent Supersonic Radial Flows*, Institute for Problems in Mechanics, Moscow Preprint No. 576.
- Raymond, J.C. & Smith, B.W., 1977, *ApJS*, 35, 419.
- Rozyczka, M., 1985, *A&A*, 143, 59.
- Rozyczka, M. & Tenorio-Tagle, G., 1985a, *A&A*, 147, 202.
- Rozyczka, M. & Tenorio-Tagle, G., 1985b, *A&A*, 147, 209.
- Samarskii, A.A. & Sobol, I.M. 1963, *Zhurnal Vichislitel'noi Matematiki i Matematicheskoi Fiziki*, 3, 702.
- Sawada, K., Shima, E., & Matsuda, T., 1989, *Mem. Fac. Eng. Kyoto Univ.*, 51, 124.
- Walder, R. & Folini, D., 1996, *A&A*, 315, 265.
- Weaver, R., McCray, R., Castor, J., Shapiro, P., & Moore, R., 1977, *ApJ*, 218, 377.
- Wrigge, M., Wendker, H.J., & Wisotzki, L., 1994, *A&A*, 286, 219.
- Yanenko, R., 1967, *Metodi drodnh shagov resheniya mnogomernih zadach matematicheskoi fiziki*, Nauka, Novosibirsk.
- Zel'dovich, Ya. B. & Raizer, Yu. P. 1967, *Physics of Shock Waves and High Temperature Hydrodynamic Phenomena*, Academic Press, New York.
- Zhukov, V.T., Zhabrodin, A.V., & Feodoritova, O.B., 1993, *Zhurnal Vichislitel'noi Matematiki i Matematicheskoi Fiziki*, 33, No. 8, 1240.